An Efficient Approach For Medical Image Fusion Using Sparse Representation Model

[1,2]S.Pradeep Kumar Reddy,[3]Dr R.V Krishnaiah,[4]Dr Y Rajasree Rao

[1]Research Scholar,Jawaharlal Nehru Technological University,Hyderabad.
[2]Assistant Professor, Vidya Jyothi Institute of Technology, Aziz Nagar, C B Post, Hyderabad.
[3]Professor&Principal,Chebrolu Engineering College, Chebrolu, Guntur,A.P.
[4]Professor,Lord Institute of Engineering &Technology, Himayath Sagar, Golconda(Post),Hyderabad.

Abstract – Multimodal Medical Image Sensor Fusion provides better visualization by integrating the image information from different medical image modalities. It plays a vital role in the precise diagnosis of very critical diseases in medical field. Generally, images acquired from different imaging modalities are downgraded due to noise interference that leads to false diagnosis in medical images. This paper presents a fusion framework for MRI-PET images, that captures the subtle details of an input images. First, the input images are decomposed by Non-Sampled Shearlet Transform (NSST) into low frequency (L_F) and high frequency (H_F) components to separate the basic and edge details. Second, the sparse representation-based model is used to merge the $L_F$components and $H_F$components are fused with Gradient-Domain Guided filtering approach. Finally, the reconstruction of fused images is employed using inverse NSST. The experimental results based on MRI and PET images database shows that the proposed approach produces good visually fused medical images with better computation measures.

1. Introduction

Nowadays, the image fusion technology is preferred to convey the image information received from various sensors [1]. Therefore, a fused single image is the outcome of this technique. The ultimate aim of image fusion technique is to combine the information of acquired images from a multi-sensor system. Here, the provided by a single camera is for a single scene alone. But, the fused image provides comprehensive information about the entire scene. In medical field, different images are taken from X-ray, Computed Tomography (CT), Magnetic Resonance Imaging (MRI), etc. In case of patients with critical diseases, none of the images is able to deliver the redundant information in accurate. This leads to more time consumption, high cost, and manual errors. Hence, the authors are initiated to develop a decision support system to diagnose the critical system using image fusion [2]. Normally, the modality of medical imaging is separated into anatomical and functional imaging. Initially, Non-Sampled Shearlet Transform is implemented to decompose the input image into approximate and detailed components [3]. Later, the sparse representation-based model is used to merge the L_F and H_F components is employed [4]. In the further step, optimization is proposed inorder to generate the weighted maps. Finally, the reconstruction of fused images is achieved using inverse NSST[5]. The results are analyzed using current image fusion methods.

2. Literature Review

In previous literatures, medical image fusion models are developed according to the pixel and feature characters. Under pixel type, to categories like spatial and transform based approaches are followed [6]. Initially, spatial method is presented by taking the average of the image regions and reference image pixels. There are few advantages like, quick processing, low complexity and clear information makes the spatial method quit superior. But, there exist some disadvantages like, poor contrast and spectral distortion. Besides, under transform based approach, the overall information is preserved, thus the transform based approach has dominated over the spatial method. Still, the limitations such as spatial inconsistency and luminance difference made the researchers to emerge new techniques.

Paisson et al.[7] presented a model using wavelet transform and principal component analysis, here, different fusion rules are applied based on the visibility and variance. The limitations of wavelet transform is overcome by multi-scale decomposition in WT [8] and wavelet packets are also adopted in [9]. This decomposition provides better image quality and localization. Though, it is superior over WT, a number of diagnostic information is missing which leads to a redundant statistics. Srinivasa et al. [10] enumerated a contourlet decomposition in image fusion based on the local energy which can produce high dimensionality curve shapes and contourlet transform (CNT). Commonly, CVT and CNT methods may face shift invariance problems that may further cause a ringing effect in the obtained fused image.

Yang et al. [11]introduced a NSCT based approach using fuzzy pulse coupled neural network. This method will suppress the spectral distortion for better image perception fusion quality. Lf and Hf decomposed components are fused using Sum Modified Laplacian (SML) and Gabor energy respectively. It showed better

results with reduced artifactscompared to WT. But in case of practical applications, NSCT is time consuming and complex. In [12] , sparserepresentation approach which is suitable for multi focus images. It reduces the computational complexity and enhances the quality of the image. The disadvantages like lack of spatial information and high reconstruction error made the researchers to develop a mew algorithm for image fusion model.

Accordingly a methodology was proposed based on NSST and sparse representation model which is used to fuse a grayscale image and a color image. Fusing such functional and anatomical images is a typical situation. Normally, in medical imaging the functional images such as PET and SPECT images are found to be as pseudo color images. Hence, it should be treated as color images with RGB channels during the fusion process. The optimal way of fusing gray scale and color image is by merging the gray scale image with each channel of the color image independently and then combining the three fused channels to construct an RGB image. However, this procedure may cause some color distortion problems. Therefore an effective approach is proposed through some color space transform methods. In which it separates the brightness or luminance component from the color image. In this method, the YUV color space is applied to accomplish the issues in grayscale and color image fusion.

3.   Proposed System

The methodologies and their concepts of the proposed fusion model is constructed and discussed in this section. The overview of the proposed system is depicted in Figure 1. Before applying NSST, the image should be processed with color space transform methods. In such a way the YUV space encodes a color image into one luminance component Y and two chrominance components U and V. This approach is quite popular and an effective tool for anatomical and functional image fusion. Ultimately, this fusion scheme contains the following three steps. First, the Y, U, and V channels are obtained by converting RGB color space to YUV color space. Then,the proposed fusion scheme is implemented to fuse the grayscale image and the Y channel of YUV color space. Finally, by performing inverse YUV conversion (YUV to RGB) over the fused Y channel, the original U channel, and the original V channel, an original color fused image is obtained. The input images PET and MRI along with the YUV and Y component image is depicted in Figure 2.
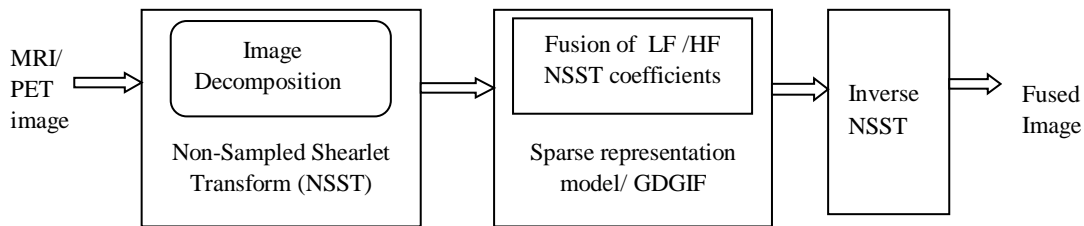

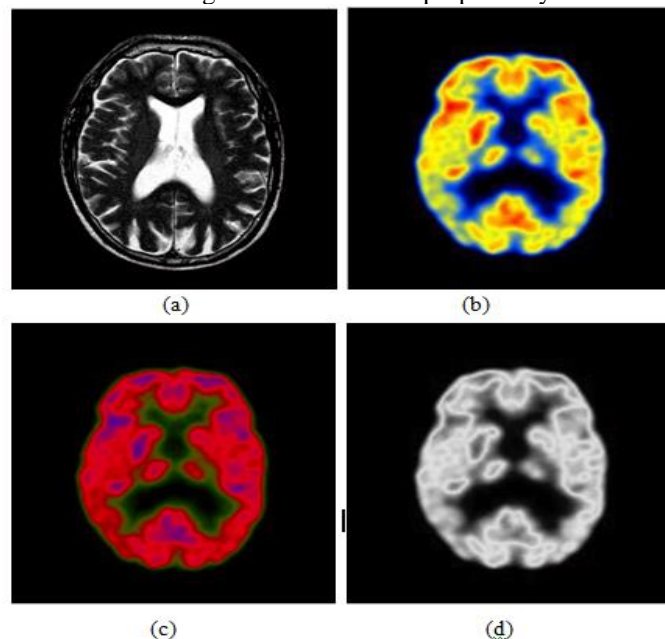Figure 1. Overview of proposed system

Figure 2 (a) MRI Image (b) PET Image (c) YUV Image (d) Extracted Y Component

3.1 NSST

The NSST is an advanced version of contourlet and wavelet transform. Therefore, it can capture the complex image contours in several dimension and directions. This transform can be applied for decomposition of an image into L_F and H_F subbands [13]. Moreover, it adopts for multi-scale and multi-directional. The decomposition is based on non sampledlaplacian pyramid filter (NSLP). Inorder to derive L_F and H_F sub image components,

The shearing measurements is obtained using shear filter (SF) on each subimage components. The MRI and PET images are decomposed into L_F and H_F sub image components of same size using (NSLP) filter. Furthermore, the L_F sub band is repeatedly decomposed to preserve the directional details of an image. At this stage, SF is implemented to obtain two directional subbands from H_F subimage components. The mathematical expression representing NSST is given by:

$$P_{DS} = \left\{ \psi_{abc} = |det\ det\ P\ |^{\frac{x}{2}} \psi(S^b P^a r - z) \right\} \quad (1)$$

Where, P refers to anisotropic dilation and S presents a shear matrix with a as scale, b as direction, and c as shift parameter. The output of NSST decomposition is shown in Figure 3.

$$\psi^{(0)}_{a,b,c}(r) = 2^{a\frac{3}{2}} \psi^{(0)}(S_0^b P_0^a r - c) \quad (2)\ \text{and}$$

$$\psi^{(1)}_{a,b,c}(r) = 2^{a\frac{3}{2}} \psi^{(0)}(1 P_1^a r - c) \quad (3)$$
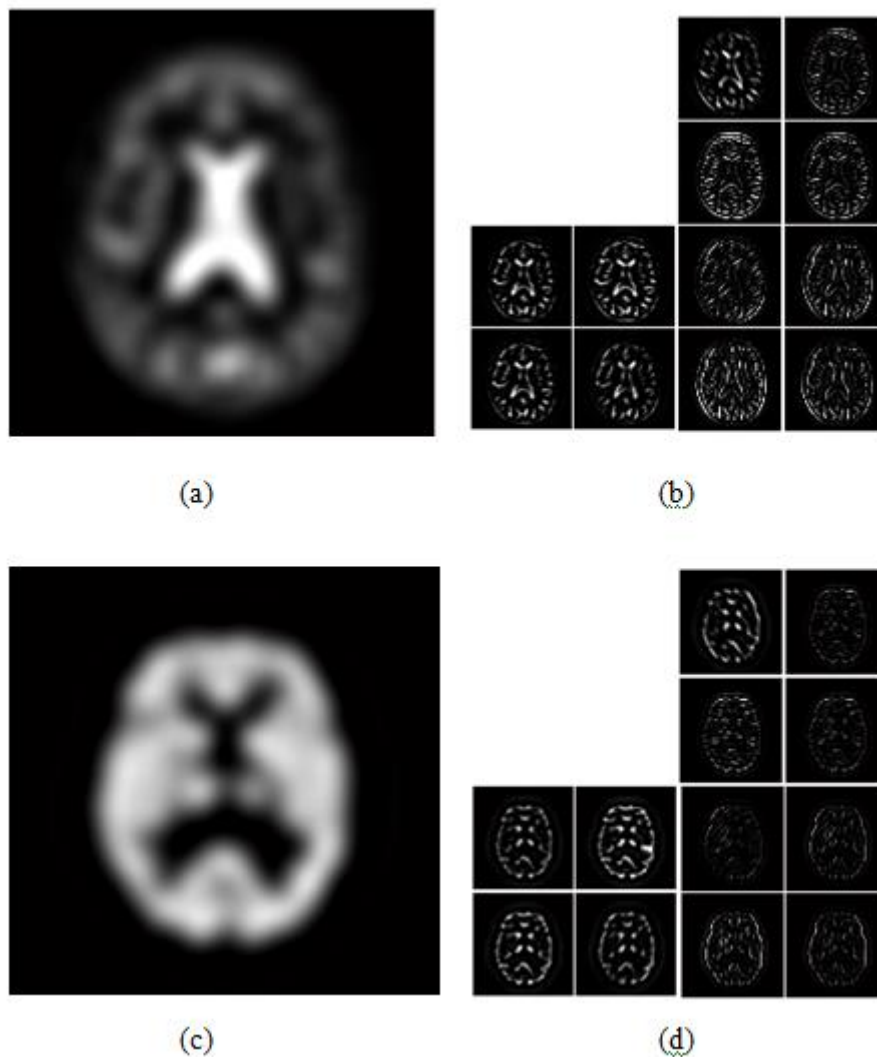

Figure 3. NSST decomposition applied on MRI and PET: (a) Low Frequency image of MRI (b) High Frequency image of MRI (c) Low Frequency image of PET (b) High Frequency image of PET

3.2 Sparse representation dictionary learning.

In SR the image data are approximated and expressed in terms of overcomplete dictionary. It can be mathematically expressed as $Y = D \times \alpha$, where, $D \epsilon R^{k \times m}$, k<m is a over complete dictionary and α represents the sparse coefficient. The optimized solution of sparse coefficient vector is computed using orthogonal matching persuit [OMP] [16]. A mock dictionary is trained from huge number of data patches during the learning stage of the dictionary. The sample training data $\{X\}_{i=1}^n$ is acquired by randomly sampling the n number of training patches of fixed size $\sqrt{k} \times \sqrt{k}$. The mathematical model of dictionary learning is expressed as $min \, d_k\{a_i^Y\}_{i=1}^a \sum_{i=1}^n \quad \|a_i^Y\|_0$ subject to $\|X - Da_i^Y\| < \epsilon$ (4)

The present fusion model is learned by the training data set of 120 PET- MRI medical images to obtain the mock dictionary. The learning process is implemented with popular K-SVD algorithm and it comprises of two steps. (1) Sparse coding using OMP to generate sparse coefficient for each image patches. (2) To find a good approximation model by dictionary updation using K-SVD [17].

The optimization equation using SVD computation is given as:

$$\min_{d_k g_k}\|C_k - d_k g_k^T\|_F^2 \, subject \, to \|d_k\|_2 = 1 \quad (5)$$

In the updation stage, the overcomplete dictionary is approximated by SVD to update the sparse coefficients. This sparse coding process is continued until best possible sparse vectors are obtained in the dictionary. The dictionary computation using SVD provides a better result for real and synthetic images by filling missing pixels for better image representation. It provides better image representation for LFcomponents. This model is fast and efficient because the sparse coefficients and pixels of the image patches are updated simultaneously during the updation of the dictionary. Finally, the LF fused image patch for two reference images PET and MRI is computed by equation. The output of sparse representation dictionary is depicted in Figure 4.

Algorithm:

Input: PET –MRI training data set $\{X\}_{i=1}^n$

Output: Learned dictionary $D^{k \times k}$

Step 1: Compute sparse vector using OMP

$min \, d_k\{a_i^Y\}_{i=1}^a \sum_{i=1}^n \quad \|a_i^Y\|_0$ subject to $\|X - Da_i^Y\| < \epsilon$

Step 2:

- ▪ The image pixels are identified from each patches
- ▪ Approximation error matrix is computed using

$$\min_{d_k g_k}\|C_k - d_k g_k^T\|_F^2 \, subject \, to \|d_k\|_2 = 1$$

- SVD (U, Δ, V) is applied column by column of approximation matrix e_k
- Update 'D' column as U
- Update 'α' by multiplying V and Δ
- Compute the updated sparse coefficient
- LF fused image patch is computed using $I_{LF} = \{D\alpha_i^f + \mu_i^A.1, if \, \alpha_i^f = \alpha_i^A \, D\alpha_i^f + \mu_i^B.1, if \, \alpha_i^f = \alpha_i^B \}$
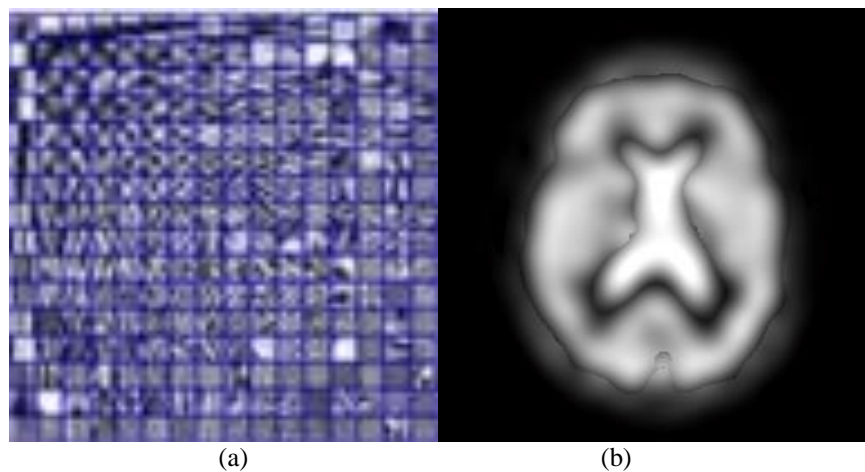

(a)   (b)

Figure 4.Output of sparse representation dictionary learning: (a) Pre-trained dictionary (b) Sparse Representation based LF fusion

3.3 Gradient domain Guided image filtering

Guided image filter is a popular linear translational variant filter for edge preservation in an image. It has lot of applications in computer vision and medical image processing for image enhancement and image fusion [14]. But, this method failed to represent the pixels near to the edges in the image. This leads to some hallows in

the output images. To reduce the hallow artifacts, a Gradient Domain Guided Image Filtering (GDGIF) was proposed by considering first-order edge- aware factor {15}. This method will represent the images more accurately near edges and thus the edge preservation is highly improved than GIF [18]. This model comprises of two steps (a) Edge-aware waiting (b) Gradient domain guided filter

3.3.1 Edge-aware waiting

Let I(x,y) be a guidance image and $\sigma_{I,1}(k)$ is the variance of I(x,y) in 3x3 window and $\sigma_{I,r}(k)$ be the variance of I(x,y) with window size of (2r+1) x (2r+1) . The mathematical model of edge-aware is given by

$$\tau_I(k) = \frac{1}{M}\sum_{i=1}^{M} \quad \frac{x(k)+\varepsilon}{x(i)+\epsilon} \quad (6)$$

The weighting function measures the importance of each pixels in the guidance image I(x,y). Also the edges are detected accurately using this edge-aware weighting.

3.3.2 Gradient domain guided filter

The GDGF provides the local linear model between I(x,y) and the filtered output A(x,y). This model preserves only the edges of the guidance image I(x,y).

$$A(i) = a_k I(i) + b_k \qquad (7)$$

The constants, a_k and b_k are obtained by the minimization of the difference between filtered output 'A' and image to be filtered 'B'

$$E = \sum_{i\in w_k} \quad [(a_k I(i) + b_{k-}B(i))^2 + \frac{\lambda}{\tau_I(k)}(a_k - \gamma_k)^2] \qquad (8)$$

$$\gamma_k = 1 - \frac{1}{1+e^{\eta(z(k)-\mu_k\alpha)}} \qquad (9)$$

The value γ_k approaches to 1 if k is an edge pixel and approaches to 0 if it is a smooth region pixel. Hence, it is less sensitivity to the selection of λ and it is set to 10^5 in this model. The optimal values of a_k and b_k are computed using

The final value of A(i) is given as eqn (10)

$$A(i) = a_i I(i) + b_i \qquad (10)$$

GDGIF operation can be represented in simple as $GDGIF_R$ (B,I) where, R is the radius of the window, B and I infer the input image and guidance image respectively.

3.4 Measurement of multiple visual feature for decision map

It is worth notable that the preservation of contrast, sharpness and structure arethe three important critical characteristics for the better visual quality of a fused image [19]. This method seperates the decision map into the three key visual feature measurement of input images as contrast saliency, sharpness and structure saliency

3.4.1 Measurement of contrast saliency

The human visual system is more sensitive to changes in the local neighbourhood pixels. Therefore the change in local contrast of each pixel is used to construct the decision map. The local contrast can be measured using simple standard deviation, computation of local neighbourhood region [20]. The measurement is done by the sliding window approach which forms a map that indicates the local contrast variation. It is expressed as:

$$LC = \left(\frac{1}{L\times P}\sum_{l=1}^{L} \quad \sum_{p=1}^{P} \quad (I(x+l,y+p) - m(x,y))^2\right)^{\frac{1}{2}} \quad (11)$$

where, m is the mean value of the window with centre (x,y) and window size of (LXP). The Contrast Saliency (CS) map is constructed by

$$CS = LC * G \qquad (12)$$

where, G is a Gaussian filter. This map provides the detail information of an image. The image pixels with high CC provides more information using the CS map. Decision map 'D$_1$' is constructed as:

$$D_1 = \{1, if\ CS = max\ 0, otherwise\ \} \qquad (13)$$

3.4.2 Measure of sharpness

Measure of sharpness is an important feature in visual perception of images. The Sum_ Modified Laplacian (SML) is preferred for sharpness measurement in spatial domain [21]. The SML cab be mathematically expressed as

$$\nabla^2_{modified}I(x,y) = |2I(x,y) - I(x-step,y) - I(x+step,y)| + $$
$$|2I(x,y) - step) - I(x,y+step)| \qquad (14)$$

By using "step=I" between the pixels, SML can accommodate more possible variations in each size. The sharpness map (SR) is defined as:

$$SR(x,y) = \sum_{m=\varphi-M_1}^{M_1} \quad \sum_{n-N_1}^{N_1} \quad [\nabla^2 I(x+m,y+n)] \qquad (15)$$

This map provides clarity information and margin mutation of an image. SR map is used to construct the decision map 'D$_2$' as;

$$D_2 = \{1, if\ SR = max\ 0, otherwise\ \} \qquad (16)$$

3.4.3 Measurement of Structure Saliency

By using local gradient covariance, structural saliency is computed to construct the decision map D$_3$. The local gradient covariance matrix is expressed as:

$$C = \left(\sum_{Y\in W}\ \ I_y^2(Y) \sum_{Y\in W}\ \ I_y(Y)I_x(Y) \sum_{Y\in W}\ \ I_y(Y)I_x(Y)\sum\ \ I_x^2(Y)\ \right) \qquad (17)$$

I$_y$(x) and I$_x$(y) denotes the gradients in x and y direction. To compute local image structure, 'C' is decomposed through eigen value as :

$$C = V(S_1^2\ 0\ 0\ S_2^2\ )V^T \qquad (18)$$

The saliency measure provides better image structure in both blurred and random noise image. The structure saliency (SS) map can be given as:

$$SS = \sqrt{(S_1 = S_2)^2 + \alpha(S_1 + S_2)^2} \qquad (19)$$

where, $\alpha > -1$, This parameter determine the corner like structures. The decision map D$_3$ is given as:

$$D_3 = \{1, if\ SS = max\ 0, otherwise\ \} \qquad (20)$$

3.4.4 GDGIF for weight map

The obtained decision maps D$_1$, D$_2$ and D$_3$ are usually not matched with object boundaries and noisy. This may produce artifacts in the fused image due to the similar brightness in the two adjacent pixels. By constructing the weight map, this halo artifacts can be avoided in fused images. Here the Guided Filtering GF) is applied on each initial decision maps D$_1$, D$_2$ and D$_3$, an optimizedweight maps are constructed which shows detailed information about the edges in an image. Two weight maps W$_1$ and W$_2$ from the source image I(x,y) with decision maps D$_1$, D$_2$ and D$_3$ are generated using the expressions:

$$W_{HF,m} = GF_1[D_m, I(x,y)] \qquad (21)$$

where, m=1,2,3 and r$_1$, r$_2$ represent the parameters of GF. The generated weight maps are based on various visual features contrast, saliency, sharpness and structure saliency measures. The overall weight map is calculated by combining these calculations of the input image I(x,y)

$$W_{HF} = \prod_{m=1}^{3}\ \ W_{HF,m} \qquad (22)$$

where, W$_{HF}$ is the resulting weight map of high frequency subbandsin the input image I(x,y).
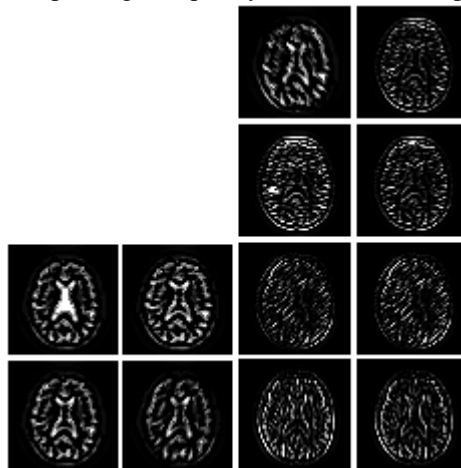

Figure 5. Output of HF fusion using GDGIF

3.5 Image Fusion

By combining the approximate and detail components in different source images, the fused image is obtained by weighted averaging of LF components decomposed from sparse coding and HF components from GDGIF. The output of GDGIF is depicted in Figure 5.

$$I_{LF} = \left\{D\alpha_i^f + \mu_i^A.1, if\ \alpha_i^f = \alpha_i^A\ D\alpha_i^f + \mu_i^B.1, if\ \alpha_i^f = \alpha_i^B\ \right\} \qquad (23)$$

$$I_{HF} = \sum_{n=1}^{N} \quad W_{HF}I(x,y) \quad (24)$$

Finally, inverse NSST is applied on the fused I_{LF} and I_{HF} images to reconstruct the resultant image F as shown in Figure 6and follows:
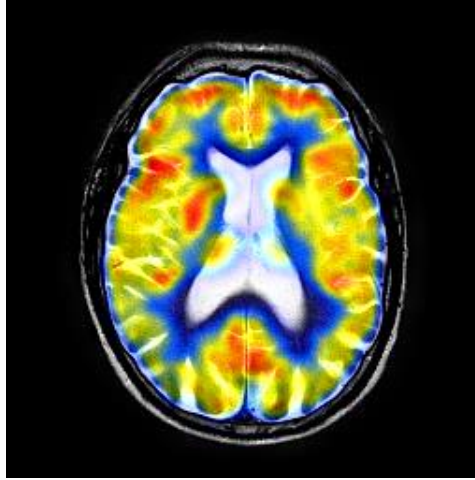
$$F = NSST^{-1}(I_{LF}^{NSST}, I_{HF}^{NSST}) \quad (25)$$

Figure 6. Output of Fused Image

4. PERFORMANCE EVALUATION

In this section, experiments are performed to verify the feasibility of our proposed method over test images and MRI medical images. Later, the results of our proposed system are compared with the existing algorithms based on GFF, CBF, NSCT-SR, NSCT-PCNN, NSCT, DWT and LP. The visual quality of an image is measured in different aspects. Here, we have considered both the quantitative and visual representation of fused images. In such a way the three commonly used fusion performance metrices are evaluated and tabulated below

A. Mutual Information: Under this evaluation metric, it conveys about how much the fused image has the information of input image. The mutual information about source image and fusion image is given by

$$MI = MI^{AF} + MI^{BF} (26)$$

where, MI^{AF} and MI^{BF} denotes the normalized information between source image and fused image.

B. Gradient based fusion metric: This measure gives the similarity between the edges exchanged from source image to fused image.

$$Q^{\frac{AB}{F}} = \frac{\sum_{i=1}^{M} \sum_{j=1}^{N} [Q^{AF}(i,j)W^{A}(i,j) + Q^{BF}(i,j)W^{B}(i,j)]}{\sum_{i=1}^{M} \sum_{j=1}^{N} [W^{A}(i,j) + W^{B}(i,j)]} \quad (27)$$

C. Structural similarity based fusion metric: It gives the quality assessment for image fusion using structural similarity technique. Structural Similarity (SSIM) is defined using the expression:

$$Q_Y = \left\{ \tau(w)SSIM\left(A, \frac{F}{w}\right) + (1 - r(w))SSIM(B, \frac{F}{w}) \text{ for } SSIM(A, B/w \geq 0.75 \ max\{SSIM\left(A, \frac{F}{w}\right), SSIM\left(B, \frac{F}{w}\right)\} \text{ for } SSIM(A, \frac{B}{w}) \leq 0.75 \right\} \quad (28)$$

Under the experimental evaluation we have prepared three set of multifocus images such as clock, lab and disk. With theseinputs the validity of our proposed method is demonstrated in Table 1. It is observed that the performance of the proposed method is better than the traditional methods. Also the obtained images in figure 5 reveal that the system has achieved a higher correlation and similarity with the source image.In this section, two groups of PET-MRI image modalities are framed. The corresponding performance comparison results are shown in Figure 6. It is observed that the proposed method has produced a clear results compared to NSCT-PCNN and CBF schemes. In medical applications, the lesion properties are more visible so that it will be more helpful for the medical experts in case of analysis and diagnosis.

Table 1 Performance measures of fused medical images

Inputs	Index	NSCT	NSCT-PCNN	NSCT-SR	CBF	GFF	Proposed method
Group 1	MI	2.557	1.306	3.050	4.890	3.268	5.361
PET-MRI	$Q^{AB/F}$	0.691	0.628	0.745	0.791	0.785	0.819
	Q^T	0.700	0.532	0.852	0.926	0.883	0.966

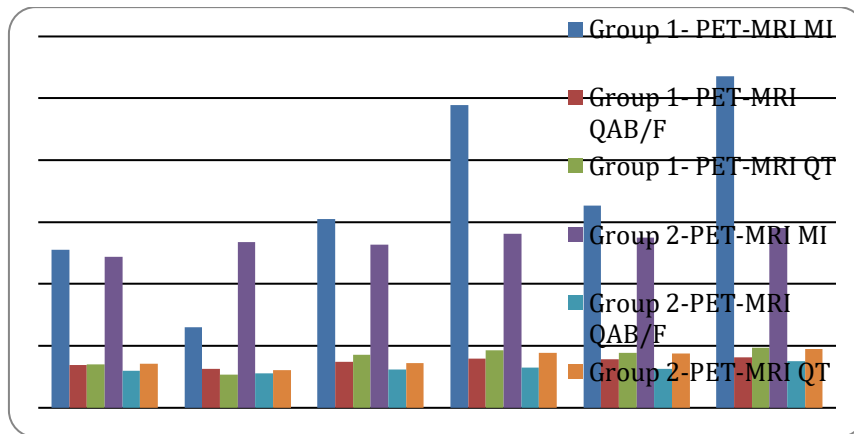| Group 2 PET- MRI	MI	2.439	2.680	2.635	2.810	2.746	2.901
	$Q^{AB/F}$	0.599	0.560	0.618	0.645	0.625	0.749
	Q^T	0.708	0.605	0.727	0.892	0.881	0.947

Figure 6 Performance comparison of Group 1 and Group 2 PET-MRI images for different methods.

5. CONCLUSION

This paper presents a medical image fusion framework based on NSST decomposition with sparse K-SVD dictionary learning.Since NSST method is employed, the shearing filters provides the spectral and spatial information through multiscale and multidirectional decomposition methods. The dictionary learning based method implied improved the detail information in low-frequency NSST subband.Furthermore, as guided filtering is applied to extract the high-frequency NSST componentsoutperforms the image fusion. Also, the color and edge details are acquired without any contamination due to artifacts. Finally, this method with seven other existing methods is executed for the PET-MRI image fusion. The experimental results highlight that the proposed system for image fusion can preserve the real and synthetic information of multiple source images better than other fusion methods.

REFERENCES

1. H. Li, X. Li, Z. Yu, and C. Mao, "Multifocus image fusion by combining with mixed-order structure tensors and multiscale neighborhood," *Information.Science.*, vol. 349, pp. 25–49, Jul. 2016.
2. Q. Zhang and M. D. Levine, "Robust multi-focus image fusion using multi-task sparse representation and spatial context," *IEEE Transactions on ImageProcessing*, vol. 25, no. 5, pp. 2045–2058, May 2016.
3. D. Gupta, "Nonsubsampled shearlet domain fusion techniques for CT–MR neurological images using improved biological inspired neural model," *Biocybernetics and Biomeical. Engineering.*, vol. 38, no. 2, pp. 262–274, 2018.
4. G. Bhatnagar, Q. M. J. Wu, and Z. Liu, "A new contrast based multimodal medical image fusion framework," *Neurocomputing*, vol. 157, pp. 143–152, Jun.'2015.
5. S. Singh, D. Gupta, R. S. Anand, and V. Kumar, "Nonsubsampled shearlet based CT and MR medical image fusion using biologically inspired spiking neural network," *Biomed. Signal Process. Control*, vol. 18, pp. 91–101, Apr. 2015.
6. Z. Liu, H. Yin, Y. Chai, and S. X. Yang, "A novel approach for multimodal medical image fusion," *Expert System and Appications.*, vol. 41, no. 16, pp. 7425–7435, 2014.
7. F. Palsson, J. R. Sveinsson, M. O. Ulfarsson, and J. A. Benediktsson, "Model-based fusion of multi- and hyperspectral images using PCA and wavelets," IEEE Transactions on Geoscience and Remote Sensing, vol. 53, no. 5, pp. 2652–2663, May 2015.
8. D. P. Bavirisetti and R. Dhuli, "Fusion of infrared and visible sensor images based on anisotropic diffusion and Karhunen–Loevetransform,"IEEE Sensors Journal, vol. 16, no. 1, pp. 203–209, Jan. 2016.
9. L. Guo, M. Dai, and M. Zhu, "Multifocuscolor image fusionbased on quaternion curvelet transform," Opt. Exp., vol. 20, no. 17,pp. 18846–18860, 2012.
10. S. Li, X. Kang, L. Fang, J. Hu, and H. Yin, "Pixel-level image fusion: A survey of the state of the art," Inf. Fusion, vol. 33, pp. 100–112, Jun. 2017.

11. Y. Yang, Y. Que, S. Huang, and P. Lin, "Multimodal sensor medical image fusion based on type-2 fuzzy logic in NSCT domain," IEEESensors Journal, vol. 16, no. 10, pp. 3735–3745, May 2016.
12. S. S. Chavan, A. Mahajan, S. N. Talbar, S. Desai, M. Thakur, and A. D'Cruz, "Nonsubsampled rotated complex wavelet transform (NSRCxWT) for medical image fusion related to clinical aspects in neurocysticercosis," Computers in Biology and Medicine, vol. 81, pp. 64–78, Feb. 2017.
13. R. Singh and A. Khare, "Fusion of multimodal medical images using Daubechies complex wavelet transform—A multiresolution approach," Inf. Fusion, vol. 19, pp. 49–60, Sep. 2014.
14. S. Aymaz, C. Köse, R. Kurban, and A. N. Toprak, "Multi-focus image fusion using stationary wavelet transform (SWT) with principal component analysis (PCA)," in Proc. 10th Int. Conference in Electrical and ElectronicsEnggineering, Nov. 2017, pp. 1176–1180.
15. H. Liu, S. Li, and L. Fang, "Robust object tracking based on principal component analysis and local sparse representation," IEEE Transactions on Instrumentation and Measurements, vol. 64, no. 11, pp. 2863–2875, Nov. 2015.
16. M. Aharon, M. Elad, and A. Bruckstein, "K-SVD: An algorithm for designing overcomplete dictionaries for sparse representation," IEEE Transactions on Signal Processing, vol. 54, no. 11, pp. 4311–4322, Nov. 2006.
17. J. A. Tropp, A. C. Gilbert, and M. J. Strauss, "Algorithms for simultaneous sparse approximation. Part I: Greedy pursuit," Signal Processing, vol. 86, no. 3, pp. 572–588, 2006.
18. F. Kou, W. Chen, C. Wen, and Z. Li, "Gradient domain guided image filtering," IEEE Transactions on. Image Processing, vol. 24, no. 11, pp. 4528–4539, Nov. 2015.
19. R. Hassen, Z. Wang, and M. M. A. Salama, "Objective quality assessment for multi exposure multifocus image fusion," IEEE Transactionson Image Processing, vol. 24, no. 9, pp. 2712–2724, Sep. 2015.
20. Z. Wang, A. C. Bovik, H. R. Sheikh, and E. P. Simoncelli, "Image quality assessment: From error visibility to structural similarity," IEEE Transactions on Image Processing, vol. 13, no. 4, pp. 600–612, Apr. 2004.
21. W. Huang and Z. Jing, "Evaluation of focus measures in multi-focus image fusion," Pattern Recognition. Letter., vol. 28, no. 4, pp. 493–500, 2007.